Biointerface Research in Applied Chemistry
Open-Access Journal (ISSN: 2069-5837)

Article
Volume 14, Issue 6, 2024, 133
https://doi.org/10.33263/BRIAC146.133

QSAR Study, Molecular Docking and Molecular Dynamic Assisted Design of Novel Quinazoline Derivatives as Anticancer Agents for Breast Cancer

Manisha Mane [1], Savita Yadav [1,*]

[1] Department of Pharmaceutical Chemistry, Bharati Vidyapeeth (Deemed to be university), Poona College of Pharmacy, Pune, 411038, India; manisha.mane09@gmail.com (M. M.); savita.yadav@bharatividyapeeth.edu (S.V.);
[*] Correspondence: savita.yadav@bharatividyapeeth.edu (S.V.);

Scopus Author ID 60107477

Received: 12.03.2024; Accepted: 7.07.2024; Published: 10.12.2024

Abstract: One of the deadly diseases affecting the global public is cancer, and more than 85% of cases are breast cancer. In the current investigation, QSAR studies have been performed on 31 analogs of the quinazoline derivatives, which have anti-proliferative activity against the cancer cell line MCF-7. The machine learning (ML)-based SVM technique exhibited a good correlation between fitted and observed biological activities. Internal and external validations have assessed and validated the descriptive and predictive performances of QSAR models. This model demonstrates an R^2 value of 0.749 and an R^2 test value of 0.991. Here, seven new molecular structures are designed using the QSAR model predictions, and their potential interaction mode with the VEGFR-2 receptor (PDB ID: 3VHE) is analyzed using molecular docking and pharmacokinetic parameters. Based on QSAR model predictions, molecular docking, dynamic, and ADMET in silico property assessments, we recommend one newly designed molecule as an anti-breast cancer drug remain further in vivo and in vitro investigations before clinical trials.

Keywords: quinazoline; breast cancer; VEGFR-2; molecular docking; ADME; molecular dynamic.

1. Introduction

According to the World Health Organization, approximately 112 nations rank cancer as the second most prevalent cause of mortality, while approximately 23 countries rank it as the third or fourth leading cause. By 2020, there will have been an estimated 9.0 million new cases of cancer reported. According to predictions, this figure will rise to 28 million instances by 2040 [1]. From a cancer perspective, breast cancer is the most prevalent and deadly malignancy. In 2020, 2.3 million women received a breast cancer diagnosis, and 684,996 of them passed away, accounting for 16% of all women's cancer deaths. In 2040, nearly three million new cases and one million deaths are expected from breast cancer [2].

Humans and other species can develop breast cancer; it starts in the breast tissue and develops from the milk ducts (ductal carcinomas) or the lobules (lobular carcinomas), which supply the ducts with milk [3]. Current breast cancer therapy regimens include the management of adjuvant drugs such as anthracyclines, epirubicin, doxorubicin, fluorouracil, and cyclophosphamide [4]. Breast cancers are classified according to the specific receptors' levels, such as the progesterone receptor, the estrogen receptor, and the human epithelial receptor 2

(HER-2). Hormone receptor status is positive in almost 75% of breast cancer patients. Unfortunately, effective treatment alternatives tailored to these subtypes are lacking [5].

Quinoxalines have been shown to be selective ATP-competitive inhibitors of several kinases, making them a valuable building block for anticancer medications [6–10]. The basic goal of anticancer medications is to neutralize cancer cells while inflicting no damage to normal cells. Many quinazoline derivatives are FDA-approved cancer treatments. Gefitinib, erlotinib, lapatinib, afatinib, and vandetanib. Gefitinib and erlotinib were used in 2003 and 2004 to treat advanced or metastatic NSCLC—the erlotinib and gemcitabine for local, advanced, or metastatic pancreatic cancer in 2005. Erlotinib acts as a tyrosine kinase inhibitor. In 2011, the FDA approved vandetanib for metastatic medullary thyroid cancer. In 2013, the afatinib for NSCLC. The FDA approved lapatinib in 2012 for breast cancer treatment [11], and it is only one drug among all quinazoline derivatives for the treatment of breast cancer. Additionally, it shows potential adverse reactions, including hair loss, a dry mouth or xerophthalmia, gastrointestinal issues such as constipation and difficulty swallowing, and dermatological conditions such as herpes simplex or aphthous ulcers. To overcome these side effects and design a potentially privileged scaffold to treat breast cancer [12].

Most recent drug discovery approaches make significant use of computational tools. Computational chemistry and *in silico* approaches were used as effective tools for drug design and discovery [13,14] with ADMETox [15] examination of new drugs. QSAR modeling is an important tool in drug development that links the chemical structures of compounds with their biological activity [16]. A ligand's biological response or activity can be predicted using different QSAR models based on its physicochemical properties.

Recently, some authors established the quinazoline derivative QSAR model for anticancer agents. In detail, HeLa cancer cell line cytotoxicity is investigated for a series (1–26) of quinazoline derivatives substituted at positions 3, 6, and 8 by QSAR-2D. Regression analyses like PCA, PLS, MLR, and MNLR, internal and external validation, and Y-randomization are used to execute, predict, and generate anti-cancer activities [17]. Another study showed the Heuristic and GEP methods to generate linear and non-linear 2D-QSAR models and CoMSIA to build 3D models with SYBYL software. Novel compounds were created using 2D-QSAR molecular descriptors and 3D contour maps. A few compounds showed optimum activity in osteosarcoma docking experiments [18]. Arjun Anant et al. are developing pharmacophore models, 3D-QSAR, and virtual screening to target CDK4/6 kinase. A total of 46 ligands were analyzed, with ADRRR_1 identified as the best pharmacophore model. The studies contribute to the future production of quinazoline derivatives targeting CDK4/6 kinase [19]. Moreover, Sagiru Hamza et al. developed a QSAR model on a quinazoline-4(3H)-one derivative using Material Studio v8.0. The model was internally and externally tested. This QSAR model was chosen for its superior statistical parameters, and seven compounds with better breast cancer activity were designed [20]. This literature review did not turn up any models created using ML techniques or new scaffolds for developing breast cancer inhibitors.

Machine learning (ML)-based QSAR techniques have been used to develop promising molecules [21]. The current study aimed to use the ML-QSAR approach to develop more effective quinazoline compounds as breast cancer inhibitors while also predicting their ADME qualities and investigating their *in silico* approach.

QSAR commonly employs SVMs due to their ability to handle high-dimensional data and non-linear relationships. The hyperplane was created to maximize separation between

classes in the feature space. SVMs thrive in QSAR applications, including drug activity, toxicity, and bioavailability prediction. These tools are versatile and robust, making them suitable for QSAR modeling. Researchers developed a framework known as "ML-QSAR" to model QSAR using machine learning approaches. SVM is a popular QSAR modeling machine learning algorithm. The framework helps choose suitable algorithms for application requirements and enhances current approaches [22,23]. The main goal of this study was to use machine learning to create a QSAR model. The model was based on more powerful quinoxaline compounds as breast cancer inhibitors and suggested new powerful candidates. Molecular docking was utilized to model and investigate their interactions with the target enzyme, verify the molecular stimulation technique, and forecast their potential pharmacological impacts.

2. Materials and Methods

2.1. Database.

This study used a database that included a number of quinoxaline derivatives. The database contained 31 compounds that are anticancer drugs and apoptosis inducers [24]. Figure 1 shows the 2D chemical structure of quinoxaline. Table 1 offers the entire set of derivatives. The compounds have been split into two subsets: 78% of the set for creating the QSAR model and 22% for validating the model. The distribution is based on activity. The activity of compounds was expressed as pIC_{50}=-logIC_{50} and was used as the dependent variable. The compounds included in the test set were chosen manually from a group of structures based on the Y-response (the dependent variable) that each exhibited. This strategy utilizes the parameter of activity as the procedure for data collection. Molecules with high activity, low activity, and moderate activity were included in both sets to guarantee even dispersion. To enhance performance, the training set was comprised of the molecules that were the most active and the least active [25].

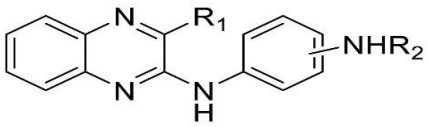

Figure 1. 2-D chemical structure of Quinoxaline scaffold.

Table 1. Structures and their corresponding IC50 and pIC_{50}.

Sr.no	R1	R2	IC_{50} (µM)	(pIC_{50})
1.	-CH3	m-(benzamide)	692.0	3.159
2.	-CH3	m-(4-chloro benzamide)	692.0	3.159
3.[b]	-CH3	m-(4-methoxy benzamide)	288.0	3.540
4.	-Cl	m-(benzamide)	5.3	5.275
5.	-Cl	m-(4-chloro benzamide)	21.4	4.669
6.[b]	-Cl	m-(4-methoxy benzamide)	380.0	3.420
7.[b]	-H	m-(4-chloro benzamide)	182.0	3.739
8.	-H	m-(4-methoxy benzamide)	219.0	3.659
9.	-CH3	p-(benzamide)	25.7	4.590
10.	-CH3	p-(4-chloro benzamide)	138.0	3.860
11.	-CH3	p-(4-methoxy benzamide)	24.0	4.619
12.	-CH3	p-(4-methyl benzamide)	60.3	4.219
13.	-Cl	p-(benzamide)	323.6	3.489
14.	-Cl	p-(4-chloro benzamide)	1000.0	3.000
15.	-Cl	p-(4-methoxy benzamide)	1000.0	3.000
16.	-CH3	p-(thiourea phenyl)	15.5	4.809
17.	-CH3	p-(phenyl) urea	13.5	4.869
18.	-CH3	p-(4-chlorophenyl) urea	9.0	5.045

Sr.no	R1	R2	IC_{50} (µM)	(pIC_{50})
19.	-CH3	p-(3-methoxyphenyl) urea	24.5	4.610
20.[b]	-CH3	p-(3-methylphenyl) urea	30.0	4.522
21.	-Cl	p-(thiourea phenyl)	170.0	3.769
22.	-Cl	p-(phenyl) urea	148.0	3.829
23.[b]	-Cl	p-(4-chlorophenyl) urea	692.0	3.159
24.[b]	-Cl	p-(3-methylphenyl) urea	64.5	4.190
25.	-Cl	p-(3-methoxyphenyl) urea	47.9	4.319
26.	-Cl	p-(4-methoxyphenyl) urea	436.5	3.360
27.	-H	p-(3-methoxyphenyl) urea	32.0	4.494
28.	-CH3	p-(4-methylbenzene) sulphonamide	22.9	4.640
29.	-CH3	p-(4-nitrobenzene) sulphonamide	10.23	4.990
30	-Cl	p-(4-methylbenzene) sulphonamide	537.0	3.270
31.	-Cl	p-(4-nitro benzene) sulphonamide	55.0	4.259

p- para; m-meta; o- orth.

2.2. Model QSAR and validation.

2.2.1. Support vector machines (SVM).

The WEKA program was used to construct 2D-QSAR models [26,27]. We created the QSAR model using the SMOreg (Sequential Minimal Optimization Regressor) approach, an effective machine learning methodology for SVM (Support Vector Machine) [28]. Regression and classification use SVMs as guided learning tools. SVM classifies data by employing a non-linear kernel function to locate hyperplanes in the high-dimensional space. This hyperplane achieves optimal separation of positive and negative variables. The support vector methodology (SVM) maximizes the margin between the hyperplane and a limited group of training data points. SVM is a common machine-learning method in cheminformatics. Several solid evaluations have highlighted SVM's use in QSPR and QSAR investigations, especially drug design. Stable, reproducible, and algorithm-independent SVM findings are its key benefits. Selecting the appropriate kernel function is crucial for a successful SVM model. Two popular kernels for classification issues are the polynomial kernel and the RBF kernel. For this study, we used a polynomial kernel instead of RBF. We used John Platt's Sequential Minimal Optimization (SMO) approach to train a support vector classifier. SMO normalizes all properties, fills gaps, and converts nominal to binary [29].

2.2.2. Internal and external model validation.

We used a cross-validation LOO (leave-one-out) to evaluate the precision of QSAR models built with partial least squares (PLS). This evaluation involved calculating the cross-validation square coefficient (q2) and the optimal number of components (ONC). To obtain the coefficient (r^2), we conducted a non-cross-validation study using the ONC that we developed during the cross-validation research. The values of r^2 and q^2 comprise the internal quality appraisal of the developed models, according to SEE (Standard Error Estimation). Equations 1 and 2 provide an outline of q^2 and r^2.

$$q^2 = \frac{\sum(y_i - \hat{y}_i)^2}{\sum(y_i - \bar{y})^2} > 0.5 \qquad (1)$$

$$r^2 = \frac{[\sum(y_i - \bar{y})(\hat{y}_i - \bar{\hat{y}})]^2}{\sum(\hat{y}_i - \bar{\hat{y}})^2 . \sum(y_i - \bar{y})^2} > 0.6 \qquad (2)$$

The model must be submitted for additional validation in accordance with the Golbraikh-Tropsha method and Roy's methodology [30–36].

Golbraikh-Tropsha's method:

$$r^2_{pred} = \frac{[\sum(y_i-\bar{y})(\hat{y}_i-\bar{\hat{y}})]^2}{\sum(\hat{y}_i-\bar{\hat{y}})^2.\sum(y_i-\bar{y})^2} > 0.6 \quad (3)$$

$$0.85 \leq K = \frac{\sum(y_i.\hat{y}_i)}{\sum(\hat{y}_i)^2} \leq 1.15 \quad (4)$$

$$0.85 \leq K' = \frac{\sum(y_i.\hat{y}_i)}{\sum(y_i)^2} \leq 1.15 \quad (5)$$

$$r^2_0 = 1 - \frac{\sum(y_i-k.\hat{y}_i)^2}{\sum(y_i-\bar{y})^2} \quad (6)$$

$$r'^2_0 = 1 - \frac{\sum(\hat{y}_i-k'.y_i)^2}{\sum(\hat{y}_i-\bar{\hat{y}})^2} \quad (7)$$

b) Roy's method:

$$r^2_m = r^2.(1-\sqrt{|r^2-r^2_0|}) \quad (8)$$

$$r'^2_m = r^2.(1-\sqrt{|r^2-r'^2_0|}) \quad (9)$$

$$\Delta r^2_m = |r^2_m - r'^2_m| \quad (10)$$

$$\overline{r^2_m} = \frac{r^2_m+r'^2_m}{2} \quad (11)$$

Other statistical quantities were calculated, such as:

$$Q^2_{F_1} = 1 - \frac{\sum_{i=1}^{n_{EXT}}(y_i-\hat{y}_i)^2}{\sum_{i=1}^{n_{Ext}}(y_i-\bar{y}_{TR})^2} \quad (12)$$

$$Q^2_{F_2} = 1 - \frac{\sum_{i=1}^{n_{EXT}}(y_i-\hat{y}_i)^2}{\sum_{i=1}^{n_{Ext}}(y_i-\bar{y}_{EXT})^2} \quad (13)$$

$$CCC = \frac{2.\sum_{i=1}^{n_{EXT}}(y_i-\bar{y}).(\hat{y}_i-\bar{\hat{y}})}{\sum_{i=1}^{n_{EXT}}(y_i-\bar{y})^2+\sum_{i=1}^{n_{EXT}}(y_{pred}-\bar{\hat{y}})^2+n_{EXT}(y_i-\bar{\hat{y}})^2} \quad (14)$$

2.3. Drug prospects and activity forecast.

Seven new ligands were proposed using the QSAR model and field contour analysis. Table 2 depicts the structures and activities of the new candidates. The results indicate that the candidate drugs being considered exhibit similar levels of activity as compound 4 and Sorafenib (Experimental activity: pIC_{50} value of 5.187).

Table 2. Newly designed compounds and their predicted activities.

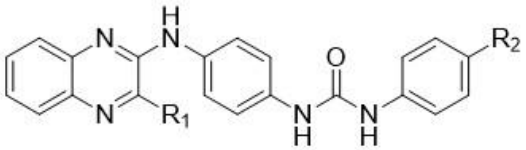

N°	R1	R2	pIC_{50}
M4	-Cl	-H	5.275[(b)]
A1	$-CO_2H$	-Cl	5.318[(a)]
A2	$-CONH_2$	-Cl	5.398[(a)]
A3	$-CH_3$	$-NH_2$	5.496[(a)]
A4	$-CH_3$	$-OC_6H_5$	5.789[(a)]
A5	$-CH_3$	$-C_6H_5$	5.409[(a)]
A6	$-CH_3$	$-CONH_2$	5.555[(a)]
A7	$-CH_3$	$-CON(CH_3)_2$	5.403[(a)]
Sorafenib	-		5.187[(b)]

pIC_{50}[(a)]: predicted activity after applying the QSAR model; pIC_{50}[(b)]: Experimental activity of the commercialized drug SOR; N° - Newly designed drug compounds; R_1, R_2 – different functional group substitution.

2.4. ADME-Tox and bioavailability.

Lipinski's rule was cast off to direct the screening of compounds[37,38]. At the initial stage of drug discovery, Lipinski's rule can be effective. It states that if a chemical violates more than two of the below criteria and calculates Log p ≤ 5, and (PSA) < 140 Å2, it is impermeable or badly absorbed [39,40]. The parameters LogP, MW, TPSA (topological polar surface area), N-violations, n-atoms, N-rot, and volume were applied to estimate drug likeliness, and the "Swiss ADME" (http://www.swissadme.ch) database was used for evaluations. The ADME and toxicity characteristics were calculated using the pkCSM-pharmacokinetics web server (http://structure.bioc.cam.ac.uk/pkcsm) [41] for analysis. All compounds are taken into consideration, and as a result, each of these seven compounds complies with the Lipinski rule and is compared with the reference standard Sorafenib. Also, toxicity profiling was performed based on the fact that compounds A3, A5, and A6 have shown toxicity, as illustrated in Tables 3 and 4. This theoretical screening helped to select a few promising active leads for consideration for further study.

Table 3. Pharmacokinetic properties and synthetic access of novel proposed compounds.

Sr. No.	Physicochemical property						Lipinski rule	Synthetic accessibility (SA)
	MW	NRB	TPSA	Log Po/w (MLogP)	HBA	HBD		
A1	461.86	8	133.31	2.69	6	4	Yes	3.13
A2	460.87	8	139.10	2.28	5	4	Yes	3.16
A3	412.44	7	122.03	2.51	4	4	Yes	3.11
A4	489.52	9	105.24	3.39	5	3	Yes	3.46
A5	473.53	8	96.010	3.64	4	3	Yes	3.45
A6	440.45	8	139.10	2.28	5	4	Yes	3.19
A7	468.51	9	116.32	4.15	5	3	Yes	3.42
Sorafenib	464.82	9	92.35	4.10	7	3	Yes	2.87
Optimal rang	<500	≤ 10	≤ 140	≤ 5	< 10	< 5	Yes/No	0 < S.A <10

MW- molecular weight**;** NRB- Num. rotatable bonds**;** TPSA- topological polar surface area**;** LogP- partition coefficient**;** HBA- Hydrogen Bond Acceptor**;** HBD- Hydrogen Bond Donor.

Table 4. Platform pkCSM-pharmacokinetics for in silico ADME/Tox prediction of novel compounds.

Drug candidate		A1	A2	A3	A4	A5	A6	A7	SOR
Absorption	Log S (SILICOS-IT)	-4.31	-4.40	-4.61	-3.62	-3.99	-4.43	-4.831	-4.496
	Log Po/w (MLogP)	2.69	2.28	2.51	3.39	3.64	2.28	4.15	5.549
	HIA (Human Intestinal Absorption) %	65.305	80.128	83.541	100	97.939	83.095	83.949	91.25
1.1Distribution	BBB (Blood–Brain Barrier)	-1.231	-1.04	-1.165	-1.222	-0.983	-1.28	-1.072	-1.741
	P-gp substrate	Yes	Yes	Yes	Yes	Yes	Yes	Yes	Yes
	Fu (Fraction unbound (human))	0	0	0.03	0.327	-0.983	0.093	0.079	0.038
Metabolism	CYP1A2 inhibitor	No	No	Yes	No	Yes	Yes	No	Yes
	CYP2C19 inhibitor	No	Yes	Yes	Yes	Yes	Yes	Yes	Yes
	CYP2C9 inhibitor	Yes	Yes	Yes	Yes	Yes	Yes	Yes	Yes
	CYP2D6 inhibitor	No	No	No	No	No	No	No	No
	CYP3A4 inhibitor	Yes	Yes	Yes	Yes	Yes	Yes	Yes	Yes
Excretion	Total Clearance (log ml/min/kg)	-0.436	-0.559	-0.09	-0.014	0.031	-0.036	0.085	-0.221
Toxicity	AMES toxicity	No	No	Yes	No	Yes	Yes	No	No
	hERG I inhibitor	No	No	No	No	No	No	No	No
	hERG II inhibitor	Yes	Yes	Yes	Yes	Yes	Yes	Yes	Yes
	H-HT (Human Hepatotoxicity)	Yes	Yes	Yes	Yes	Yes	Yes	Yes	Yes

2.5. Molecular docking.

In silico modeling is an excellent way to design drugs by anticipating possible interactions between ligands and the disease targets (receptors) [42]. The molecular docking study was carried out by the internet facility (https://cadd.labshare.cn/cb-dock2/php/blinddock.php) [43]. The most stable conformations of compounds were meticulously selected and analyzed utilizing Discovery Studio 2020 Client software version 20.1. The compounds pass the ADME and toxicity profile, and they are only selected for docking study.

2.5.1. Preparation of ligands.

During ADME analysis of the proposed compounds, those who pass pharmacokinetic testing are selected as the new proposed ligands (A1, A2, A4, and A7), and Sorafenib is the reference standard. The MM2 function of Chem3D 16.0 was utilized to create the structure's two-dimensional model. Mol2 file format is used to upload to the Swiss Dock server, and you can click on the prepare a ligand button.

2.5.2. Preparation of receptor.

The receptor (PDB ID: 3VHE) was obtained from the RCSB website in PDB format. (http://www.rscb.org) Removed the water molecules and heteroatoms from the receptor. The hydrogen atoms were introduced along with the grid box.

A grid box of 50 x 50 x 50 grid points was constructed around the active locations of VEGFR and c-Raf, with a grid spacing of 0.375. During docking, we kept the receptor rigid and the ligand flexible. The Lamarckian Genetic Algorithm was used to create the ligand output conformations. The docked conformations were then grouped further using an all-atom RMSD cut-off of 4. The clusters were further examined in terms of binding energy, ligand efficiency, inhibitor constant, intermolecular energy, van der Waals, electrostatic energies, and so on. The interaction study was performed using PyMol and Discovery Studio Visualize using the lowest binding energy conformation of the ligand. Molecular docking illustrates the ligand-receptor interactions as well as the ligands' affinity for the receptor.

In this research, Sorafenib and a new proposed ligand (A1, A2, A4, and A7) were placed in binding sites that were the same. Figure 2 shows the linked site's surface and the different ways that compounds and link sites move together.

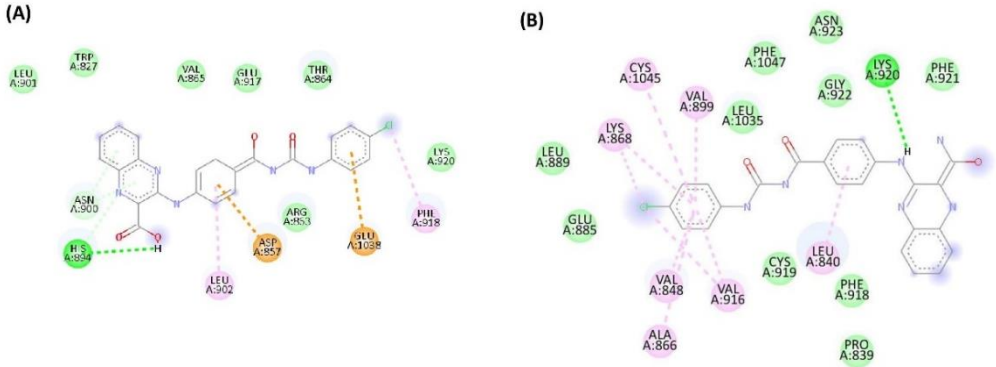

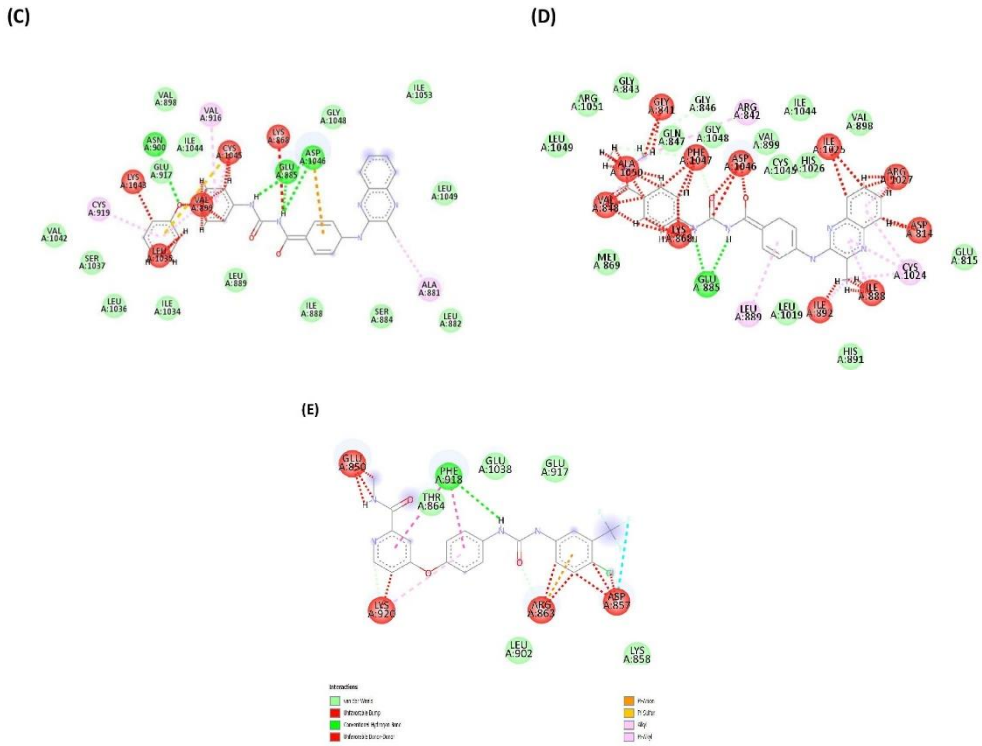

Figure 2. 2D interaction of **(A)** A1-3VHE; **(B)** A2-3VHE; **(C)** A4-3VHE; **(D)** A7-3VHE; **(E)** Sorafenib-3VHE.

Sorafenib and the newly proposed ligands (A1, A2, A4, and A7) both have negative G scores, suggesting that the receptor interacts with them spontaneously. The docking scores are displayed in Table 5.

Table 5. The Vina score of the ligand-receptor complexes studied.

Complex	A1-3VHE	A2-3VHE	A4-3VHE	A7-3VHE	SOR-3VHE
Predicted activity pIC_{50}	5.318	5.398	5.789	5.403	5.187
Vina score (kcal/mol)	-8.10	-10.2	-12.2	-11.7	-7.80

2.6. Molecular dynamics.

Further investigation was conducted using MD simulation on the ligand-protein complex that had the highest docking score. The compound A4 has the highest docking score of -12.2, and the structure is displayed in Figure 3. The Desmond software was used for the MD simulations study [44]. In order to solve the system using the OPLS 2005 force field, a water box with a volume of 10 cubic units was utilized, employing the TIP3P water model. In order to neutralize the systems, sodium ions (counter ions) were introduced. Subsequently, we used an energy gradient convergence threshold of 1 kcal.mol-1 to minimize the system. Prior to that, we used Desmond's standard six-step relaxation method for pre-equilibration. Initially, two minimization processes are carried out: one involving a constrained solute and another one without any constraints. We need to use the NPT ensemble in steps three to six to run short dynamic simulations of 12 ns, 24 ns, and 100 ns at 10, 50, 300, and 300 K, respectively. A 100 ns molecular dynamics simulation was then executed. Desmond set all other settings to their default value coordinates [44,45].

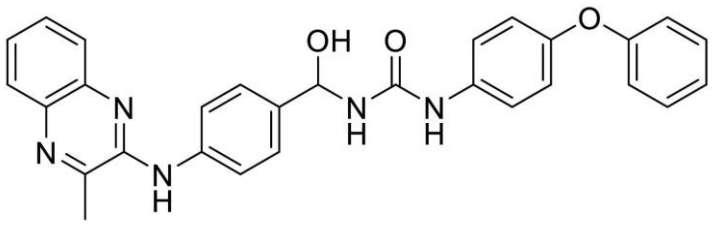

Figure 3. Chemical structure of compound A4 used for dynamic study.

3. Results and Discussion

3.1. QSAR model and their statistical analysis.

SMO regression findings were produced using a familiar technique known as sequential minimization optimization for regression (SMOreg). After examining the statistical quality criteria, it was determined that the RMSE produced by SMOreg was 0.0021. The cross-validated r^2 or (q^2) is 0.520, and the r^2 pred is 0.749 (more than 0.6), indicating that the built SVM model makes decent internal and external predictions. The mean absolute error (MAE) value of the obtained model indicates the extent of the prediction error. The training set demonstrates an MAE of 0.0019 and r^2 of 0.999, suggesting superior predictive capabilities. It is evident that SVM algorithms are useful for internal and external prediction.

The QSAR model's external validation comprises the SVM model's predicated pIC_{50} values for training and test sets. Tables 6, 7, and 8 contain these values. Additionally, Figure 4 displays a scatter plot comparing the observed values of pIC_{50} to the predicted values across both the training sets and test sets. Considering the results mentioned above, we could say that the QSAR model developed is excellent, robust, predictive, and reliable. The model was best suited to predict the activity of new anticancer compounds with confidence.

Table 6. QSAR model coefficient values after external validation.

Parameters	Validation		Threshold value
	External	Internal	
$\mathbf{r^2_{pred}}$	0.749	0.999	> 0.6
$\mathbf{r_0^2}$	0.721	0.991	Near r^2 value
$\mathbf{r_0'^2}$	0.738	0.987	Near r^2 value
K	1.019	1.000	$0.85 \leq K \leq 1.15$
K’	0.978	1.000	$0.85 \leq K \leq 1.15$
$\frac{(\mathbf{r^2 - r_0^2})}{\mathbf{r^2}}$	0.037	0.009	< 0.1
$\frac{(\mathbf{r^2 - r'^2_0})}{\mathbf{r^2}}$	0.014	0.031	< 0.1
$\mathbf{\lvert r^2 - r'^2 \rvert}$	-0.002	-0.017	< 0.3
$\mathbf{r_m^2}$	0.624	0.906	> 0.5
$\mathbf{r_m'^2}$	0.672	0.887	> 0.5
$\mathbf{\bar{r}_m^2}$	0.648	0.896	> 0.5
$\mathbf{\Delta r_m^2}$	-0.049	0.019	< 0.2
$\mathbf{Q_{F_1}}$	0.982	0.999	> 0.7
$\mathbf{Q_{F_2}}$	0.699	0.999	> 0.7
CCC	0.857	0.999	> 0.85

Table 7. The training set experimental and predicted pIC_{50} values.

Compound id	Actual	SVM	
		Predicted	Error
1.	3.159	3.16	0.001
2.	3.159	3.16	0.001
8.	3.659	3.662	0.003
10.	3.860	3.857	-0.003
11.	4.619	4.618	-0.001
12.	4.219	4.217	-0.002
13.	3.489	3.486	-0.003
14.	3.000	3.001	0.001
15.	3.000	3.001	0.001
16.	4.809	4.806	-0.003
17.	4.869	4.868	-0.001
18.	5.045	5.044	-0.001
19.	4.610	4.608	-0.002
20.	4.522	4.519	-0.003
21.	3.769	3.773	0.004
22.	3.829	3.831	0.002
23.	3.159	3.16	0.001
25.	4.319	4.32	0.001
27.	4.494	4.493	-0.001
28.	4.640	4.638	-0.002
30.	3.270	3.27	0
31.	4.259	4.256	0.003

Table 8. Test set experimental and predicted pIC_{50} values.

Comp. id	Actual	SVM	
		Predicted	Error
6 test	3.420	3.561	0.141
7 test	3.739	3.188	-0.551
20 test	4.522	4.519	-0.003
23 test	3.159	3.16	0.001
24 test	4.190	3.982	-0.208

Figure 4. An activity plot of training and test set pIC_{50}s versus predictions.

3.2. Drug candidates and activity prediction.

Seven novel derivatives are designed from a derived QSAR model. Some structural variations exist in these newly proposed compounds. Diaryl ureido linkage is more significant for anticancer action when comparing these newly proposed compounds to existing derivatives. Tables 3 and 4 show the pharmacokinetic and ADMET properties of the developed quinazoline derivatives. With the exception of one criteria violation (MW > 500), the developed analogs have all met Lipinski's rule of five; hence, drug-like qualities are likely. Compounds with

synthetic accessibility are ranked from 1 (easy synthesis) to 10 (difficult synthesis). These compounds have synthetic accessibility ratings of 2.87 to 3.46, indicating a simple synthesis. The proposed compounds have uniform brain distribution and can permeate the central nervous system, according to LogBB and LogPS values. They also function as substrates and inhibitors of superenzyme 3A4, the most important category for drug metabolism. Total clearance (TC) is a measure that shows the relationship between bodily substance content and elimination rate per unit of time. These inhibitors have reasonable TC values for the body's drug compound. Studies on toxicity indicate that AMES is safe; however, compounds A3, A5, and A6 exhibit AMES toxicity and should not be considered for further study. As a result, all proposed compounds follow the Lipinski rule, and the newly proposed compounds A3, A5, and A6 have a toxicity profile given in Tables 3 and 4.

3.3. Analysis of docking study.

Molecular docking is a method for identifying probable link conformations between drugs and receptors. In this study, the new proposed ligands A1, A2, A4, A7, and Sorafenib were inserted into the corresponding receptor binding sites (PDB ID: 3-VHE). We have identified and observed five compounds, each occupying a unique binding pocket. Table 9 displays the compounds' docking scores, as well as their amino acid residues.

Table 9. Ligand-Receptor (PDB ID: 3-VHE) docking results.

Sr. No	Name of Compound	Predicted IC_{50} value	Docking Score	Hydrogen bonds
1	A1	5.318	-8.10	His894
2	A2	5.398	-10.2	Lys920
3	A4	5.789	-12.2	Gly885, Asp1046, Asn900
4	A7	5.403	-11.7	Gly885, Asp1046
5	Sorafenib	5.187	-7.80	Phe918

All selected ligands and the reference drug interact spontaneously with receptors that have negative G scores. Due to their considerable affinity, the ligands A4 and A7 show higher docking scores than the reference ligand on the active side.

3.4. Dynamics simulation study.

3.4.1. RMSF and RMSD.

Figure 5 shows the results of a root mean square deviation (RMSD) study on the simulation trajectories to determine the stability of the ligand-receptor complexes.

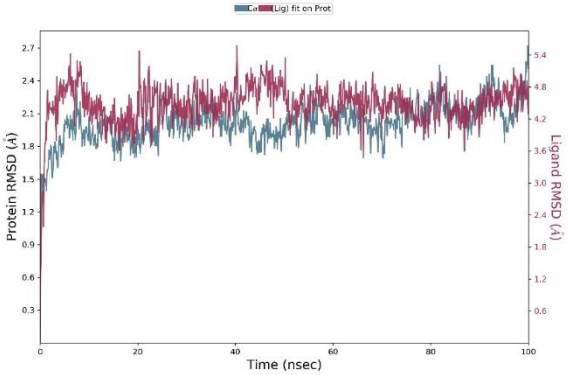

Figure 5. Protein and ligand RMSD values generated by a 100ns MD simulation.

The RMSD value changes over time in Figure 5 for the receptor backbone (3VHE), the ligand (A4), and the whole complex structure (A4-3VHE). The backbone RMSD for the enzyme (3VHE) complex (A4-3VHE) was very stable from the beginning to the end, with almost no change. The complex (A4-3VHE) backbone's RMSD went up from 40 to 60 ns, then stayed the same until the exercise was over. The receptor backbone's RMSD is typical of globular values for these complexes, which means it stayed pretty steady during the MD simulation.

The RMSF study is a good way to talk about changes in certain parts of protein chains, like how stable the amino acid residues are, especially those that are found in active site binding. The intensity of the changes stayed below 2.0 A° showen in Figure 6.

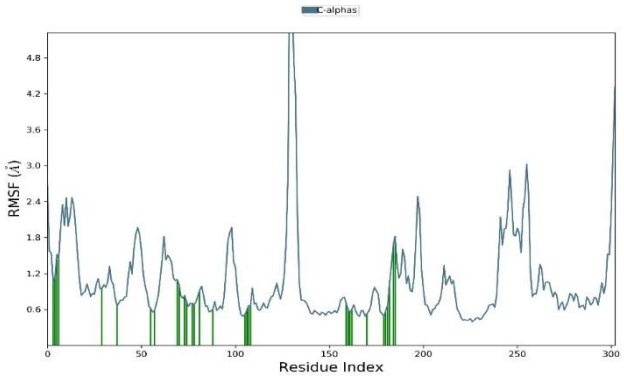

Figure 6. Desmond software simulation of A4-3VHE protein RMSF with ligands for 100 ns.

The residues that interact with the ligand are highlighted by green vertical lines in the graph. Upon analysis, it is evident that none of these interacting residues exhibit major fluctuations throughout the simulation, indicating a relatively stable interaction between the ligand and these specific residues.

However, it is important to note that the loop region spanning residues 110-120 is inherently highly flexible. This flexibility is reflected in the higher fluctuations observed in this region compared to other parts of the protein. The increased mobility in this loop region might contribute to the overall dynamics of the ligand binding. Still, it does not appear to disrupt the key interactions as indicated by the stable RMSD of the interacting residues.

The stability of the complex is further supported by the tiny variations in the RMSF plots and the comparatively lower RMSD values of the A4 compound, which are all below 3 Å.

3.4.2. Protein-ligand contacts.

During the simulation, the interactions between the simulated ligands and amino acid residues through thoroughly examining the MD analysis, as shown in Figure 7. The histogram in Figure 8 displays the interactions between the protein residues and the ligand, confirming the formation of specific bonds like hydrogen, hydrophobic interactions, and water-bridged hydrogen bonds. Compound A4, for instance, formed a hydrogen bond and demonstrated the maintenance of the simulation time with specific interactions, including GLN-885 (120%), ASP-1046 (50%), and CYS-817 (10%). Water bridge contacts were also seen with ASP-814 (90%), ILE-1025 (70%), and some protein residues (GLU-815, CYS-817, VAL-899, HIS-1026, ARG-1027, and ILE-1044) that kept the simulation time below 20%. Additionally, we observed hydrophobic bonds with ILE-888 (75%), VAL-916 (70%), LEU-1035 (60%), and ALA-866 (55%).

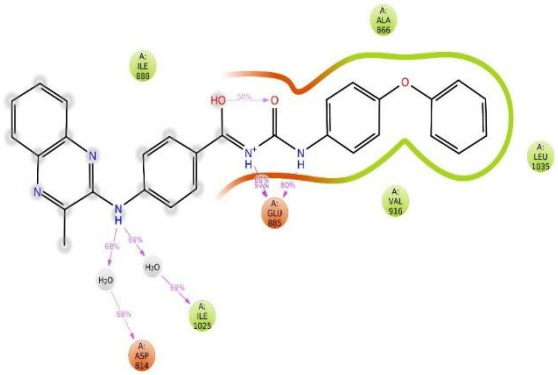

Figure 7. A diagram to demonstrate protein residue-ligand atom interactions.

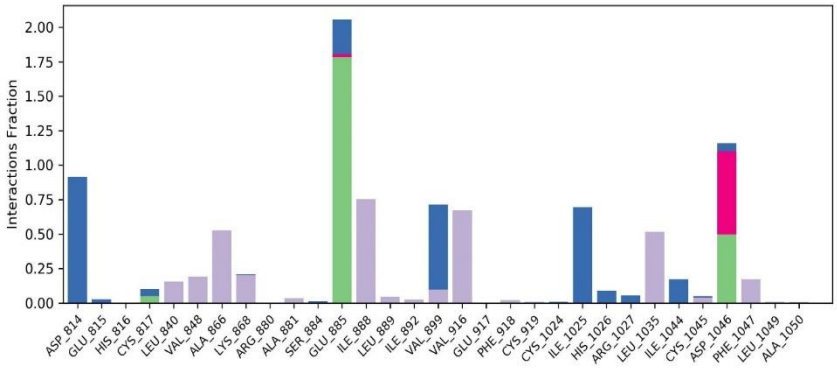

Figure 8. The protein-ligand interactions of the ligands with 3VHE during 100 ns MD.

3.4.3. Ligand properties (rGyr, MolSA, SASA, and PSA).

Additional properties, including radius of gyration (rGyr), solvent accessible surface area (SASA), polar surface area (PSA), and molecular surface area (MolSA), were used to analyze the ligand characteristics. The rGyr descriptor quantifies the RMSD at the center of mass of a molecule throughout the simulation. Angstroms are used to calculate the Desmond MD algorithm. When a molecule is flexible, it can change its shape more often, which affects how stable it is in a simulation timeline. Figure 8 shows that rGyr values ranged from 6.5 to 7.0 Å, with an average of 6.77 Å for the A4 molecule.

Another molecular descriptor studied is MolSA, which represents molecular boundaries and governs interactions with surrounding molecules and the environment. Figure 9 depicts MolSA's Vander Waal surface. It assists in identifying steric conflicts and other non-bonded interactions.

SASA (solvent-accessible surface area) measures a molecule's solvent-accessible, wide-open surface area. The SASA study reveals ligand binding and protein folding. During simulations, monitoring SASA changes can reveal molecular surface area evolution, system dynamics, and conformational changes. The usual values were 140 Å. The surface area (PSA) of molecules includes charged polar atoms and functional groups. PSA describes a molecule's solubility, permeability, and polar interactions. PSA is important because highly polar molecules struggle to permeate cellular membranes. Figure 8 demonstrates that potential compounds had acceptable PSA and had a value of 148 Å.

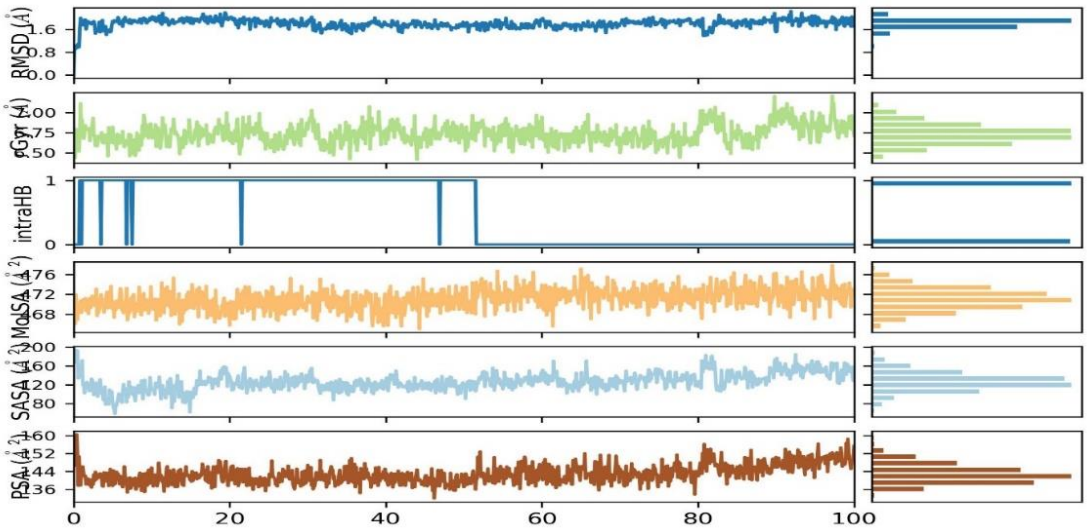

Figure 9. Properties of the Ligand A4 with (PDB ID: 3VHE) 100 ns simulation.

All investigated ligand (A4) properties indicate that the complexes remained stable throughout the simulation.

4. Conclusions

The current study successfully accomplished its objective by employing various computer-based drug design methodologies. It suggests novel pharmaceutical compounds that have improved anticancer activity compared to drugs like Sorafenib that are currently on the market. Using the 2D-QSAR method, an extensive examination was conducted on a group of quinoxaline-based molecules that have demonstrated significant potential in therapeutic anticancer treatments. We successfully developed predictive models that met rigorous internal and external validation criteria by leveraging this correlation. After analyzing the contour maps, seven drug candidates were identified that demonstrated enhanced activities compared to the reference drug Sorafenib. It is thought that new compounds with a diaryl ureido linkage are better for anticancer activity than existing derivatives. Diaryl ureido is crucial in designing anticancer molecules due to its near-perfect binding with certain acceptors. Alkylating pharmacophores are linked to high-affinity DNA binders and type II inhibitors, including RAF, KDR, and Aurora kinases. In type II inhibitors, this moiety makes one or two hydrogen bonds with a conserved glutamic acid and the DFG motif's aspartic acid backbone amide, and it is confirmed by an in-silico study".

The findings predict all the molecules investigated in silico as drugs, adhering to Veber and Lipinski's rules. They fulfill the majority of the criteria specified in the ADME data. Because of the molecular docking analysis results, candidate A4 is the most stable within the receptor (PDB ID: 3VHE). A molecular dynamic simulation analysis was conducted on the A4-3VHE complex to verify the molecular docking method's outcomes. This analysis involved binding the A4 compound and the receptor (PDB code: 3VHE) for a duration of 100 ns. Our research aims to enhance and improve these A4 molecules to pave the way for future therapeutic developments. The positive computational results enhance the wet lab synthesis of the proposed ligand A4 and its derivatives for cancer therapy.

Funding

The authors would like to thank the Chhatrapati Shahu Maharaj Research, Training, And Human Development Institute (SARTHI), Government of Maharashtra, for financial support. File no. SARTHI/Fellowship/CSMNRF-2021/2021-22/896. Year 2022.

Acknowledgments

We are grateful to the "Bharati Vidyapeeth (Deemed to be university), Poona College of Pharmacy, Pune." (AMCT) for its pertinent help concerning the programs.

Conflicts of Interest

The authors declare that the research was conducted in the absence of any commercial or financial relationship that could be construed as a potential conflict of interest.

References

1. Elkaeed, E. B.; Yousef, R. G.; Khalifa, M. M.; Ibrahim, A.; Mehany, A. B. M.; Gobaara, I. M. M.; Alsfouk, B. A.; Eldehna, W. M.; Metwaly, A. M.; Eissa, I. H.; El-Zahabi, M. A. Discovery of New VEGFR-2 Inhibitors: Design, Synthesis, Anti-Proliferative Evaluation, Docking, and MD Simulation Studies. *Molecules* **2022**, *27*, 6203, https://doi.org/10.3390/molecules27196203.
2. Alneyadi, A.; Nizami, Z. N.; Aburawi, H. E.; Hisaindee, S.; Nawaz, M.; Attoub, S.; Ramadan, G.; Benhalilou, N.; Al Azzani, M.; Elmahi, Y.; Almeqbali, A.; Muhammad, K.; Eid, A. H.; Vijayan, R.; Iratni, R. Synthesis of New Chromene Derivatives Targeting Triple-Negative Breast Cancer Cells. *Cancers (Basel)* **2023**, *15*, 2682, https://doi.org/10.3390/cancers15102682.
3. Sergiusz L.; Marcin C.; Alicja F.; Jacek B.; Robert S.; Andrzej S. Breast Cancer-Epidemiology, Risk Factors, Classification, Prognostic Markers, and Current Treatment Strategies -An Updated Review. Cancer, 2021, 13, 4287, https://doi.org/10.3390/cancers13174287 Aruchamy, B.; Kuruburu, M. G.; Bovilla, V. R.; Madhunapantula, S. V.; Drago, C.; Benny, S.; Presanna, A. T.; Ramani, P. Design, Synthesis, and Anti-Breast Cancer Potential of Imidazole–Pyridine Hybrid Molecules In Vitro and Ehrlich Ascites Carcinoma Growth Inhibitory Activity Assessment In Vivo. *ACS Omega* **2023**, *8*, 40287–40298, https://doi.org/10.1021/acsomega.3c04384.
4. Sharma, D.; Kumar, S.; Narasimhan, B. Estrogen Alpha Receptor Antagonists for the Treatment of Breast Cancer: A Review. *Chem. Cent. J.* **2018**, *12*, 107, https://doi.org/10.1186/s13065-018-0472-8.
5. Buravchenko, G. I.; Shchekotikhin, A. E. Quinoxaline 1,4-Dioxides: Advances in Chemistry and Chemotherapeutic Drug Development. *Pharmaceuticals* **2023**, *16*, 1174, https://doi.org/10.3390/ph16081174.
6. Kethireddy, S.; Ketha, S.; Eppakayala, L.; Chithaluri, S. Anti-Cancer Docking Investigations of Quinoxaline Phenyl Thiazolidinones. *Vietnam Journal of Chemistry* **2022**, *60*, 346–353, https://doi.org/10.1002/vjch.202100146.
7. Badithapuram, V.; Nukala, S. K.; Thirukovela, N. S.; Dasari, G.; Manchal, R.; Bandari, S. Design, Synthesis, and Molecular Docking Studies of Some New Quinoxaline Derivatives as EGFR Targeting Agents. *Russ J Bioorg Chem* **2022**, *48* , 565–575, https://doi.org/10.1134/S1068162022030220.
8. Zayed, M. F. Chemistry, Synthesis, and Structure Activity Relationship of Anticancer Quinoxalines. *Chemistry* **2023**, *5*, 2566–2587, https://doi.org/10.3390/chemistry5040166.
9. Ismail, M. M. F.; Shawer, T. Z.; Ibrahim, R. S.; Abusaif, M. S.; Kamal, M. M.; Allam, R. M.; Ammar, Y. A. Novel Quinoxaline-3-Propanamides as VGFR-2 Inhibitors and Apoptosis Inducers. *RSC Adv* **2023**, *13*, 31908–31924. https://doi.org/10.1039/d3ra05066a.
10. Shagufta; Ahmad, I. An Insight into the Therapeutic Potential of Quinazoline Derivatives as Anticancer Agents. *Medchemcomm* **2017**, *8*, 871–885, https://doi.org/10.1039/c7md00097a.
11. Ando, K.; Wada, T.; Cao, X. Precise Safety Pharmacology Studies of Lapatinib for Onco-Cardiology Assessed Using in Vivo Canine Models. *Sci Rep* **2020**, *10*, 738, https://doi.org/10.1038/s41598-020-57601-x.

12. Suleimen, Y. M.; Metwaly, A. M.; Mostafa, A. E.; Elkaeed, E. B.; Liu, H. W.; Basnet, B. B.; Suleimen, R. N.; Ishmuratova, M. Y.; Turdybekov, K. M.; Van Hecke, K. Isolation, Crystal Structure, and in Silico Aromatase Inhibition Activity of Ergosta-5, 22-Dien-3 β -Ol from the Fungus Gyromitra Esculenta. *J Chem* **2021**, *2021*, 5529786, https://doi.org/10.1155/2021/5529786.
13. El-Adl, K.; Sakr, H. M.; Yousef, R. G.; Mehany, A. B. M.; Metwaly, A. M.; Elhendawy, M. A.; Radwan, M. M.; ElSohly, M. A.; Abulkhair, H. S.; Eissa, I. H. Discovery of New Quinoxaline-2(1H)-One-Based Anticancer Agents Targeting VEGFR-2 as Inhibitors: Design, Synthesis, and Anti-Proliferative Evaluation. *Bioorg Chem* **2021**, *114*, 105105, https://doi.org/10.1016/j.bioorg.2021.105105.
14. Moukhliss, Y.; Koubi, Y.; Alaqarbeh, M.; Muzzammel Rehman, H.; Maghat, H.; Sbai, A.; Bouachrine, M.; Lakhlifi, T. Computational and Retrosynthetic Investigation of Isoxazole-Bearing Chalcones as Antioxidant Activate Compounds. *ChemistrySelect* **2023**, *8*, e202203908, https://doi.org/10.1002/slct.202203908.
15. Shahlaei, M. Descriptor Selection Methods in Quantitative Structure-Activity Relationship Studies: A Review Study. *Chemical Reviews. American Chemical Society* **2013**, *113*, 8093–8103, https://doi.org/10.1021/cr3004339.
16. Kasmi, R.; Hadaji, E.; Bouachrine, M.; Ouammou, A. QSAR and Molecular Docking Study of Quinazoline Derivatives as Anticancer Agents Using Molecular Descriptors. *Mater Today Proc* **2022**, *51*, 1821–1830, https://doi.org/10.1016/J.MATPR.2020.05.283.
17. Lian, Z.; Sang, C.; Li, N.; Zhai, H.; Bai, W. 3D,2D-QSAR Study and Docking of Novel Quinazolines as Potential Target Drugs for Osteosarcoma. *Front Pharmacol* **2023**, *14*, 1124895, https://doi.org/10.3389/fphar.2023.1124895.
18. Anant, A.; Ali, A.; Ali, A.; Gupta, G. D.; Asati, V. A Computational Approach to Discover Potential Quinazoline Derivatives against CDK4/6 Kinase. *J Mol Struct* **2021**, *1245*, 131079, https://doi.org/10.1016/J.MOLSTRUC.2021.131079.
19. Abdullahi, S. H.; Uzairu, A.; Shallangwa, G. A.; Uba, S.; Umar, A. B. Ligand-Based Drug Design of Quinazolin-4(3H)-Ones as Breast Cancer Inhibitors Using QSAR Modeling, Molecular Docking, and Pharmacological Profiling. *J Egypt Natl Canc Inst* **2023**, *35*, . https://doi.org/10.1186/s43046-023-00182-3.
20. Lo, Y. C.; Rensi, S. E.; Torng, W.; Altman, R. B. Machine Learning in Chemoinformatics and Drug Discovery. *Drug Discovery Today*. **2018**, *23*, 1538–1546, https://doi.org/10.1016/j.drudis.2018.05.010.
21. Nekoei, M.; Mohammadhosseini, M.; Pourbasheer, E. QSAR Study of VEGFR-2 Inhibitors by Using Genetic Algorithm-Multiple Linear Regressions (GA-MLR) and Genetic Algorithm-Support Vector Machine (GA-SVM): A Comparative Approach. *Medicinal Chemistry Research* **2015**, *24*, 3037–3046, https://doi.org/10.1007/s00044-015-1354-4.
22. Niazi, S. K.; Mariam, Z. Recent Advances in Machine-Learning-Based Chemoinformatics: A Comprehensive Review. *International Journal of Molecular Sciences*. **2023**, *24*, 11488, https://doi.org/10.3390/ijms241411488.
23. El Newahie, A. M. S.; Nissan, Y. M.; Ismail, N. S. M.; Abou El Ella, D. A.; Khojah, S. M.; Abouzid, K. A. M. Design and Synthesis of New Quinoxaline Derivatives as Anticancer Agents and Apoptotic Inducers. *Molecules* **2019**, *24*, 1175, https://doi.org/10.3390/molecules24061175.
24. Shameera Ahamed, T. K.; Rajan, V. K.; Muraleedharan, K. QSAR Modeling of Benzoquinone Derivatives as 5-Lipoxygenase Inhibitors. *Food Science and Human Wellness* **2019**, *8*, 53–62, https://doi.org/10.1016/j.fshw.2019.02.001.
25. Hall, M.; Frank, E.; Holmes, G.; Pfahringer, B.; Reutemann, P.; Witten, I.H. The WEKA Data Mining Software: An Update. *ACM SIGKDD explorations newsletter* **2009**, *11*, 10-18.
26. Abdulfatai, U.; Ejeh, S.; Ajala, A.; Adawara, S. N.; Babatunde, O. S.; Ya'u Ibrahim, Z. QSAR, Molecular Docking, and Molecular Designs of Some Anti-Epilepsy Compounds. *Intelligent Pharmacy* **2023**, *2*, 427-434, https://doi.org/10.1016/j.ipha.2023.11.011.
27. Cortes, C.; Vapnik, V.; Saitta, L. Support-Vector Networks. *Machine Learning* **1995**, *20*, 273-297.
28. Jagat S. C.; Sandeep K. D.; Deepak S.; Subhash M. A.; Gajendra P. S. QSAR-Based Models for Designing Quinazoline/Imidazothiazoles/Pyrazolopyrimidines Based Inhibitors against Wild and Mutant EGFR. PLoS One, **2014**, 9, 7, e101079. doi: https://doi.org/10.1371/journal.pone.0101079.
29. Moukhliss, Y.; Khatabi, K. El; Koubi, Y.; Maghat, H.; Sbai, A.; Bouachrine, M.; Lakhlifi, T. 2D-QSAR Modeling of Novel Pleconaril Derivatives (Isoxazole-Based Molecules) as Antiviral Inhibitors against Coxsackievirus B3 (CVB3). *Jordan Journal of Pharmaceutical Sciences* **2021**, *14*, 137-156.
30. El fadili, M.; Er-rajy, M.; Imtara, H.; Noman, O. M.; Mothana, R. A.; Abdullah, S.; Zerougui, S.; Elhallaoui, M. QSAR, ADME-Tox, Molecular Docking and Molecular Dynamics Simulations of Novel Selective

Glycine Transporter Type 1 Inhibitors with Memory Enhancing Properties. *Heliyon* **2023**, *9*, e13706, https://doi.org/10.1016/j.heliyon.2023.e13706.
31. Aloui, M.; Er-rajy, M.; Imtara, H.; Goudzal, A.; Zarougui, S.; El fadili, M.; Arthur, D. E.; Mothana, R. A.; Noman, O. M.; Tarayrah, M.; Menana, E. QSAR Modelling, Molecular Docking, Molecular Dynamic and ADMET Prediction of Pyrrolopyrimidine Derivatives as Novel Bruton's Tyrosine Kinase (BTK) Inhibitors. *Saudi Pharmaceutical Journal* **2024**, *32*, 101911, https://doi.org/10.1016/j.jsps.2023.101911.
32. Rosell-Hidalgo, A.; Young, L.; Moore, A. L.; Ghafourian, T. QSAR and Molecular Docking for the Search of AOX Inhibitors: A Rational Drug Discovery Approach. *J Comput Aided Mol Des* **2021**, *35*, 245–260, https://doi.org/10.1007/s10822-020-00360-8.
33. Golbraikh, A.; Wang, X.S.; Zhu, H.; Tropsha, A. Predictive QSAR Modeling: Methods and Applications in Drug Discovery and Chemical Risk Assessment. In Handbook of Computational Chemistry, Leszczynski, J., Ed.; Springer Netherlands: Dordrecht, **2016**; pp. 1-48, https://doi.org/10.1007/978-94-007-6169-8_37-3.
34. Mandloi, D.; Dabade, S. J.; Bajaj, A. V; Atre, H. Molecular Docking and QSAR Studies for Modeling Antifungal Activity of Triazine Analogues against Therapeutic Target NMT of Candida Albicans. *International Journal of Pharmaceutical Sciences and Drug Research* **2020**, *13*, 140–146, https://doi.org/10.25004/ijpsdr.2021.130204.
35. Faris, A.; Ibrahim, I. M.; Alnajjar, R.; Hadni, H.; Bhat, M. A.; Yaseen, M.; Chakraborty, S.; Alsakhen, N.; Shamkh, I. M.; Mabood, F.; M. Naglah, A.; Ullah, I.; Ziedan, N.; Elhallaoui, M. QSAR-Driven Screening Uncovers and Designs Novel Pyrimidine-4,6-Diamine Derivatives as Potent JAK3 Inhibitors. *J Biomol Struct Dyn* **2023**, 1-30, https://doi.org/10.1080/07391102.2023.2283168.
36. Singhal, S.; Khanna, P.; Misra, N.; Khanna, L. Multitarget Diallyl Disulfides (DADS) against Aβ Aggregation: Screening through Molecular Docking with Aβ42 & ZnII-Aβ16, ADME, DFT & Synthetic Strategy. *ChemistrySelect* **2021**, *6*, 4112–4123, https://doi.org/10.1002/slct.202004635.
37. Lipinski, C. A. Lead- and Drug-like Compounds: The Rule-of-Five Revolution. *Drug Discovery Today: Technologies*.**2004**, *1*, 337–341, https://doi.org/10.1016/j.ddtec.2004.11.007.
38. Daina, A.; Michielin, O.; Zoete, V. SwissADME: A Free Web Tool to Evaluate Pharmacokinetics, Drug-Likeness and Medicinal Chemistry Friendliness of Small Molecules. *Sci Rep* **2017**, *7*, 42717, https://doi.org/10.1038/srep42717.
39. Umar, A.B.; Uzairu, A.; Shallangwa, S.U.G.A. In Silico Studies of Some Potential Anti-Cancer Agents on M19-MEL Cell Line. *Moroccan J. Chem.* **2021**, *9*, https://doi.org/10.48317/IMIST.PRSM/morjchem-v9i2.20575.
40. Pires, D. E. V.; Blundell, T. L.; Ascher, D. B. PkCSM: Predicting Small-Molecule Pharmacokinetic and Toxicity Properties Using Graph-Based Signatures. *J Med Chem* **2015**, *58*, 4066–4072, https://doi.org/10.1021/acs.jmedchem.5b00104.
41. Forli, S.; Huey, R.; Pique, M. E.; Sanner, M. F.; Goodsell, D. S.; Olson, A. J. Computational Protein-Ligand Docking and Virtual Drug Screening with the AutoDock Suite. *Nat Protoc* **2016**, *11*, 905–919, https://doi.org/10.1038/nprot.2016.051.
42. Liu, Y.; Yang, X.; Gan, J.; Chen, S.; Xiao, Z. X.; Cao, Y. CB-Dock2: Improved Protein-Ligand Blind Docking by Integrating Cavity Detection, Docking and Homologous Template Fitting. *Nucleic Acids Res* **2022**, *50*, W159–W164, https://doi.org/10.1093/nar/gkac394.
43. Shoaib, T. H.; Abdelmoniem, N.; Mukhtar, R. M.; Alqhtani, A. T.; Alalawi, A. L.; Alawaji, R.; Althubyani, M. S.; Mohamed, S. G. A.; Mohamed, G. A.; Ibrahim, S. R. M.; Hussein, H. G. A.; Alzain, A. A. Molecular Docking and Molecular Dynamics Studies Reveal the Anticancer Potential of Medicinal-Plant-Derived Lignans as MDM2-P53 Interaction Inhibitors. *Molecules* **2023**, *28*, 6665, https://doi.org/10.3390/molecules28186665.
44. Bouzina, A.; Bouone, Y. O.; Sekiou, O.; Aissaoui, M.; Ouk, T. S.; Djemel, A.; Mansouri, R.; Ibrahim-Ouali, M.; Bouslama, Z.; Aouf, N. E. In Vitro Antitumor Activity, Molecular Dynamics Simulation, DFT Study, ADME Prediction, and Eg5 Binding of Enastron Analogues. *RSC Adv.* **2023**, *13*, 19567–19584, https://doi.org/10.1039/d3ra02904b.